

Validation of visible/near-IR atmospheric absorption and solar emission spectroscopic models at 1 cm^{-1} resolution

Dan Lubin,¹ Andrew Vogelmann,¹ Pamela J. Lehr,^{1,2} Ann Kressin,³
James Ehamjian,⁴ and V. Ramanathan¹

Abstract. A Fourier transform infrared (FTIR) spectrometer, operating at 1 cm^{-1} resolution between 9000 and $24,669\text{ cm}^{-1}$ ($0.405\text{--}1.111\ \mu\text{m}$) has been used to check the spectral composition of databases that form the basis for most atmospheric absorption parameterizations used in climate models, remote sensing, and other radiative transfer simulations. The spectrometer, operating near sea level under clear skies, obtained relative atmospheric transmission measurements of the direct solar beam by means of a heliostat. The spectroscopic data were compared with a line-by-line radiative transfer model (LBLRTM) calculation of direct solar beam flux, which used as input data a monochromatic model extraterrestrial solar flux spectrum currently in common use. This intercomparison revealed that the extraterrestrial solar flux spectrum contains 266 solar absorption features that do not appear in the data, resulting in an excess of approximately 1.92 W m^{-2} in the model's solar constant. The intercomparison also revealed 97 absorption features in the data that do not appear in the HITRAN-96 database as used by LBLRTM, resulting in a model underestimate of shortwave absorption of $\sim 0.23\text{ W m}^{-2}$ for a solar zenith angle of 42° . These small discrepancies revealed by the intercomparison indicate that current extraterrestrial solar irradiance models and spectroscopic databases used by shortwave atmospheric radiative transfer models are nearly entirely complete for purposes of atmospheric energy budget calculation. Thus clear or cloudy sky "excess absorption" is unlikely to be related to an incomplete identification of atmospheric absorbing gases and their spectroscopic features, at 1 cm^{-1} resolution, for a clean troposphere of normal composition.

1. Introduction

Climate modeling, remote sensing and other shortwave atmospheric radiative transfer applications require accurate databases of the spectroscopic line parameters, and the extraterrestrial solar source function. Scrutinizing the databases in use is particularly timely for resolving the debate surrounding excess absorption, in which many studies indicate that observed atmospheric absorption is systematically underestimated by model calculations (see reviews by *Stephens and Tsay* [1990] and *Ramanathan and Vogelmann* [1997]). Under closer examination, models have been shown to be missing absorption features found in clear-sky spectra, such as those associated with the effects of oxygen collision pairs at visible and near-infrared wavelengths [*Pfeilsticker et al.*, 1997; *Solomon et al.*, 1998; *Mlawer et al.*, 1998; *Michalsky et al.*, 1999]. The radiative impact of these absent bands is only 1–2% of the atmospheric solar absorption [*Zender*, 1999], which is too small to explain a significant amount of the excess absorption. However, this indicates the benefit and need for closely examining the spec-

tral details of atmospheric absorption, which may point toward species or chemical processes that are absent from our models [e.g., *Solomon et al.*, 1999; *Daniel et al.*, 1999].

In this paper we examine the databases of spectroscopic line parameters and the extraterrestrial solar source function using a high-resolution spectrum (1 cm^{-1}) which spans 9000–24,669 cm^{-1} ($0.405\text{--}1.111\ \mu\text{m}$). The spectrum, obtained from a Fourier transform infrared (FTIR) spectrometer, is compared to calculations by a state-of-the-art line-by-line radiative transfer algorithm. This study provides information that is complementary to the studies cited above due to the combination of the high resolution available and wide spectral region investigated. Thus we will be able to investigate features at this high resolution for this critical spectral region that contains 67% of the total extraterrestrial solar source function. The objective of these intercomparisons are as follows (1) determine if there are any solar absorption features in the extraterrestrial solar irradiance spectrum which do not appear in the spectrometer measurements, and (2) determine if there are any absorption features in the measurement that do not appear in the model calculation.

2. Methodology

Relative direct solar beam transmission spectra were measured using a Bomem model DA-8 Fourier transform infrared (FTIR) spectrometer configured for a resolution of 1 cm^{-1} . The principles and important practical aspects of FTIR spectrometry can be found in the work of *Griffiths and de Haseth* [1986]. In the FTIR instrument used for this study, the interferometer path difference is selectable, such that a resolution

¹Center for Clouds, Chemistry, and Climate and Center for Atmospheric Sciences, Scripps Institution of Oceanography, La Jolla, California.

²Now at Space Sciences Laboratory, University of California, Berkeley.

³Department of Chemistry, Miramar College, San Diego, California.

⁴Biospherical Instruments, Inc., San Diego, California.

Copyright 2000 by the American Geophysical Union.

Paper number 2000JD900317.
0148-0227/00/2000JD900317\$09.00

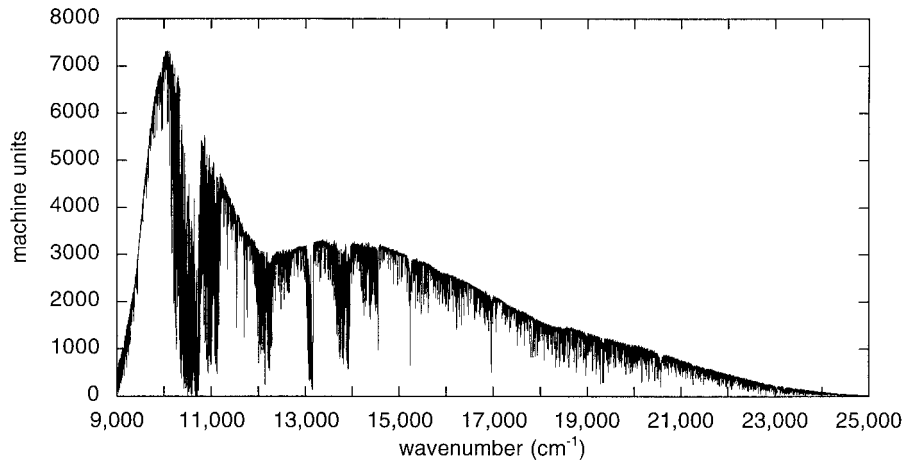


Figure 1. A spectrum of the direct solar beam flux, without radiometric calibration, measured by the FTIR spectrometer at 1 cm^{-1} resolution, in La Jolla, California, under a clear sky on August 31, 1998.

of 0.12, 1, 2, 4, or 16 cm^{-1} can be chosen. With this particular instrument, we find that a resolution of 1 cm^{-1} gives the best compromise between the ability to identify narrow absorption features and the ability to use a suitably short integration time over which the atmospheric composition is unlikely to change significantly. The spectrometer utilized a quartz beam splitter and a room-temperature silicon detector, which enabled a wavelength coverage of 0.405 to $1.111 \mu\text{m}$ ($24,669\text{--}9000 \text{ cm}^{-1}$), with band limit wavelength resolutions of 0.016 and 0.123 nm, respectively. A plane-mirror heliostat was used to track the Sun and to image the direct solar beam onto the spectrometer's entrance aperture. Neutral density filters, a copper aperture 0.5 mm in diameter, and an iris diaphragm, were used at the entrance aperture to protect the spectrometer from the intensity of the direct solar beam. Each measured spectrum consists of 100 coadded interferometer scans, for a total integration time of ~ 5 min. The data were reduced from raw interferograms to relative flux spectra (machine units) using simple Bartlett (triangular) apodization [Griffiths and de Haseth, 1986]. These spectra were collected during the August and September 1998, under clear-sky conditions at the Scripps

Institution of Oceanography, on the coast of southern California. Atmospheric transmissivity was sampled through relatively clean air masses moving inland from the Pacific Ocean.

Figure 1 shows a spectrum obtained on August 31, 1998, exhibiting one of the highest signal-to-noise ratios. An adequate signal-to-noise ratio was often difficult to obtain with this instrument due to the frequent passage of low clouds, fog, and haze overhead. Rapidly changing sky conditions would either suddenly reduce the gain from that initially set using the iris diaphragm or would suddenly increase the signal to the point of detector saturation. The spectrum of Figure 1 is chosen for the model intercomparison presented here because during this measurement the detector gain was monitored as constant throughout the integration time. The upper envelope of this spectrum is a complicated curve with a maximum near $10,000 \text{ cm}^{-1}$. This envelope represents the transmitted solar beam flux reaching the spectrometer, weighted by the spectral reflectances of the interferometer's optical elements, the spectral transmissivity of the neutral density filter, and the detector responsivity. Several thousand absorption features are seen at this resolution, and several well-known water vapor and oxygen

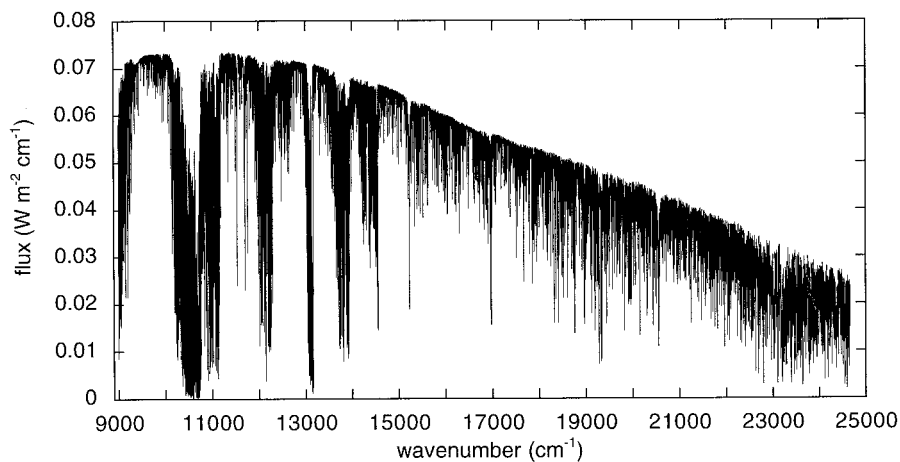


Figure 2. A model estimate of the direct solar beam spectral irradiance, at 1 cm^{-1} resolution, using LBLRTM with the molecular absorption database discussed in the text. The calculations include Rayleigh scattering and use the Kurucz model extraterrestrial solar irradiance. The calculation is for clear skies and for the same solar zenith angle as the measurement of Figure 1 (42°).

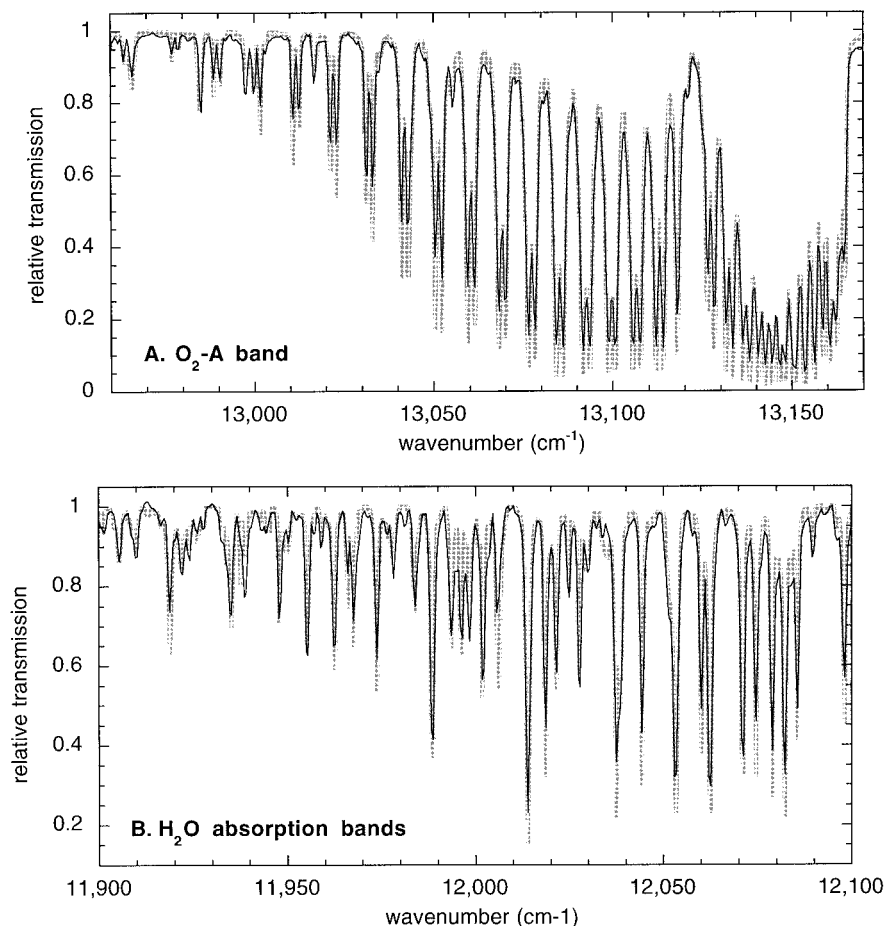


Figure 3. A comparison of the measurement from Figure 1 and the model spectrum of Figure 2 (both normalized to unity at their upper envelopes), in (a) the oxygen-A band and (b) part of an H₂O absorption band. The measurement is shown by the narrow black line, and the model calculation is shown by the thicker gray line.

absorption bands can be identified, respectively, around 10,500, 12,000, and 13,100 cm⁻¹. Although the spectrometer can function to wavenumbers as large as 25,000 cm⁻¹, as seen in Figure 1, the largest wavenumbers (24,670–25,000 cm⁻¹) are omitted from our model intercomparisons due to an unacceptably low signal-to-noise ratio.

For comparison with the most commonly used atmospheric databases this observed spectrum is compared to that computed using the line-by-line radiative transfer model (LBLRTM) [Clough and Iacono, 1995]. We use the recently released update of LBLRTM, version 5.10, which inputs a new line parameter database that incorporates recent corrections by Giver *et al.* [2000] with the HITRAN-96 database [Rothman *et al.*, 1998]. LBLRTM computes the gaseous absorption optical depths at the resolution of the HITRAN database (0.001 cm⁻¹) using all 32 absorbers available from the database. The atmospheric structure and profiles of molecular concentrations are obtained from a McClatchey model midlatitude summer profile contained in LBLRTM. As will be shown below, LBLRTM with this model atmosphere profile gives atmospheric transmissions that are in very good qualitative agreement with the FTIR measurements in various well-known water vapor bands; this agreement is good enough for the absorption feature identification exercises reported herein. The spectrum of direct beam solar irradiance at the Earth's

surface is computed from these absorption optical depths by including the Rayleigh scattering optical depth, and an extra-terrestrial solar source function. The solar source function used is the most recent version of the Kurucz monochromatic, full disk, extraterrestrial solar irradiance spectrum (obtained from <http://www.arm.gov/docs/research/sw.html>). This spectrum is based on solar photospheric modeling validated in part by interferometer measurements made at Kitt Peak Observatory [Kurucz, 1992]. To make this calculation comparable to our spectrometer measurement, the scanning function for Bartlett apodization has been applied, using a maximum path difference of 0.6 cm⁻¹, which is the path difference that would result in an ideal interferometer yielding a resolution of 1 cm⁻¹. The direct beam solar flux calculation that matches the measurement of Figure 1 is shown in Figure 2.

For the intercomparison the upper envelopes of the model calculation and measurement are normalized to unity in 104 wavenumber intervals between 9000 and 24,669 cm⁻¹. The upper envelopes used for the normalization are determined for each interval by locating all inflection points within the spectra and keeping the half of the inflection points that reside at the greatest unnormalized values (thereby seeking the upper rather than the lower envelope). These points are then screened iteratively where points are removed if they are lower than one standard deviation from their computed mean; this

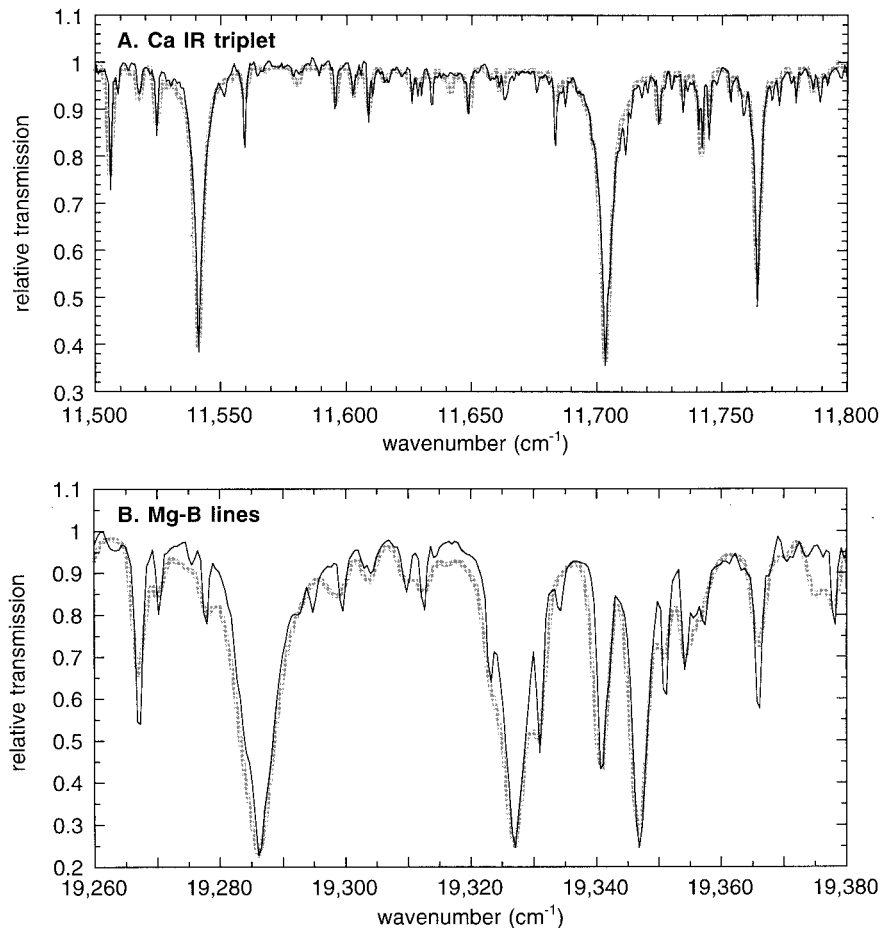


Figure 4. A comparison of the measurement of Figure 1 and the Kurucz model tabulation of extraterrestrial solar irradiance (both spectra normalized to unity at their upper envelopes) in the wavenumber regions containing the well-known Fraunhofer lines of (a) the Ca IR triplet and (b) the Mg-B lines. The measurement is shown by the narrow black line, and the Kurucz spectrum is shown by the thicker gray line.

procedure is repeated until less than 20% of the points remain. A final screen removes all points outside plus/minus one standard deviation from the mean. The upper envelope used for normalization is the mean of the surviving points.

Because we have no direct radiometric calibration of the spectrometer measurements, our intercomparison is thus limited to the identification of absorption lines and features at 1 cm^{-1} resolution. There is some information in the large discrepancies found in the strengths of some absorption lines, but we cannot comprehensively evaluate the accuracy of the entire HITRAN database without radiometric calibration. Nor can we evaluate the accuracy of various treatments of continuum absorption, as the continuum present in the real atmospheric absorption cannot be separated from the instrument's response function. Similarly, spectral features having widths of the order of 1 nm , such as the O_2 dimer [Michalsky *et al.*, 1999], will not be discernable in our data given the need to curve-fit to the instrument response function.

3. Results

In Figure 3 we show the general agreement between the normalized data and the normalized LBLRTM direct beam calculation, in two well-known atmospheric absorption features. In Figure 3a, covering the oxygen-A band, the spectrom-

eter resolves all of the major absorption features; although in the LBLRTM calculation, the features are relatively larger. This is due to the slight resolution mismatch between the data and the LBLRTM calculations, which is intentional: our LBLRTM calculation is processed to the resolution of an ideal interferometer configured for a resolution of 1 cm^{-1} , while the measured spectrum is at a slightly coarser resolution due to the (Bartlett) apodization required for real interferometer data. Having the model calculation at a slightly higher spectral resolution will be helpful to explain some of the more complicated features seen in the measured spectra (i.e., resolution of doublets, or superimposed solar and telluric features). The slightly higher resolution of the model calculation will result in its absorption features being generally deeper than the measurement, provided that all atmospheric properties are the same or comparable between the model and the real atmospheres.

In Figure 3b we demonstrate the agreement between the LBLRTM calculation and the measurement in a portion of well-known water vapor absorption band ($11,900\text{--}12,100 \text{ cm}^{-1}$). The overall agreement is very good, again with most of the model water vapor absorption features appearing deeper in the model calculation. Between $11,990$ and $12,005 \text{ cm}^{-1}$ there are two measured features that illustrate the usefulness of having the model calculation at a slightly higher resolution: the

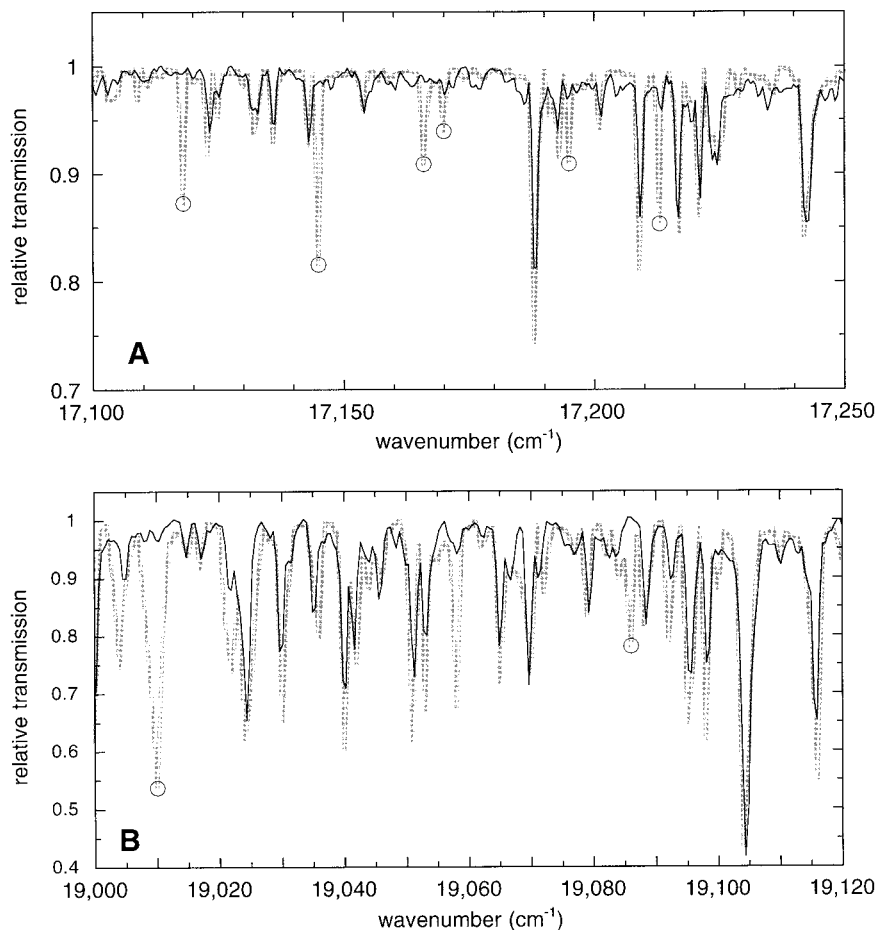


Figure 5. Examples of solar absorption features in the Kurucz 1 cm^{-1} spectrum which do not appear in the spectrometer measurement (a) in the wavenumber interval $17,100\text{--}17,250\text{ cm}^{-1}$ and (b) in the wavenumber interval $19,000\text{--}19,120\text{ cm}^{-1}$. The measurement is shown by the narrow black line, and the Kurucz spectrum is shown by the thicker gray line. The unrealized solar absorption features are highlighted by circles at their local minima.

model calculation shows how the measured multiplet and doublet are resolved into discrete absorption features (lines). This type of feature resolution has proven useful throughout the absorption line identification exercise we have undertaken here. The LBLRTM calculation of Figure 3b was done with a generic midlatitude summer relative humidity profile, for the same solar zenith angle as the measurement (42° , averaged over the integration time), and no attempt was made to adjust the model water vapor column to match the absorption line strengths to the measurement.

In Figure 4 we compare a spectrometer measurement directly with the tabulation of the Kurucz [1992] extraterrestrial solar irradiance spectrum (no radiative transfer calculation). We can do this in the various atmospheric window regions, the purpose being to identify solar absorption features that appear in the Kurucz [1992] tabulation but do not appear in the data. However, in Figure 4 we first examine some well-known strong solar features, to demonstrate the quality and wavelength accuracy of the FITR measurement. The solar spectrum is tabulated in increments of 1 cm^{-1} . This means that the effective spectral resolution of the narrowest solar absorption features in this tabulation will be of the order of $2\text{--}3\text{ cm}^{-1}$ (full width at half maximum). Thus there is a spectral mismatch between the LBLRTM radiative transfer simulation of atmospheric optical

depths, and the extraterrestrial solar irradiance spectrum that is used as input data for the entire radiative transfer calculation. The extraterrestrial solar irradiance spectrum by itself has an effective resolution of $2\text{--}3\text{ cm}^{-1}$, while the total radiative transfer calculation is done at 0.001 cm^{-1} resolution and is subsequently reduced to a resolution slightly finer than the FITR measurement using the Bartlett apodization function discussed above. The resolution mismatch between the FITR measurement and the extraterrestrial solar irradiance spectrum can be seen in many of the smaller solar features in the two panels of Figure 4, while for the larger well-known solar absorption features (Ca-IR triplet and Mg-B lines), there is excellent agreement between the tabulation and the measured spectrum. Figure 4 illustrates how wavelength calibration accuracy can easily be ascertained using the larger solar absorption features.

4. Conclusions

We now intercompare the observed and modeled spectra to search for discrepancies. An examination of the signal-to-noise ratio throughout the entire wavenumber range of our measurements suggests that we can reliably perform these line identification exercises for all absorption features having a center

Table 1. Spectral Features in the Extraterrestrial Solar Irradiance Spectrum Which Do Not Appear in the FTIR Spectrum

Wavenumber	Relative Feature Depth	Solar Irradiance, $\text{mW m}^{-2} \text{cm}^{-1}$
9239	0.88	64.84
9505	0.94	69.33
9588	0.94	69.61
9817	0.88	64.93
9836	0.88	65.03
11283	0.79	59.23
11642	0.92	68.78
11645	0.94	70.61
12035	0.85	63.77
12567	0.94	69.67
12725	0.74	54.75
12773	0.89	65.80
12906	0.84	62.21
12941	0.93	68.62
13193	0.95	69.75
13223	0.90	66.40
13332	0.92	67.83
13377	0.89	65.81
13548	0.92	67.37
13997	0.89	64.86
14031	0.92	66.55
14141	0.88	63.86
14224	0.93	67.24
14445	0.91	64.96
14572	0.93	66.38
14582	0.88	63.10
14591	0.93	66.39
14704	0.89	63.33
14722	0.92	65.35
14738	0.87	61.71
14777	0.93	66.02
14834	0.87	61.76
14868	0.94	66.72
15001	0.95	67.43
15025	0.94	66.06
15038	0.93	65.72
15040	0.88	61.90
15073	0.91	64.20
15090	0.93	65.39
15289	0.90	63.03
15358	0.94	65.51
15462	0.87	60.18
15496	0.94	64.98
15517	0.94	65.21
15639	0.86	59.52
15656	0.86	59.01
15698	0.88	60.91
15728	0.94	64.69
15734	0.86	59.33
15960	0.90	61.20
16032	0.91	61.98
16068	0.88	59.70
16196	0.94	63.57
16231	0.79	53.41
16297	0.94	63.49
16310	0.82	54.89
16344	0.92	61.63
16369	0.81	54.59
16541	0.94	62.62
16580	0.83	55.26
16867	0.77	50.74
17001	0.92	60.60
17027	0.91	59.52
17118	0.87	56.93
17145	0.82	53.16
17166	0.91	59.20
17170	0.94	61.19
17195	0.91	59.17
17213	0.85	55.49
17327	0.87	56.26

Table 1. (continued)

Wavenumber	Relative Feature Depth	Solar Irradiance, $\text{mW m}^{-2} \text{cm}^{-1}$
17370	0.91	58.54
17417	0.91	58.87
17421	0.91	58.96
17427	0.92	59.58
17553	0.88	56.12
17561	0.89	56.81
17573	0.85	54.45
17600	0.89	56.72
17608	0.89	56.90
17618	0.90	57.22
17684	0.89	56.74
17728	0.88	55.90
17747	0.87	55.44
17784	0.77	48.65
17898	0.84	52.84
17903	0.84	52.76
17917	0.89	56.17
17932	0.83	52.27
17935	0.83	52.30
17955	0.91	57.10
17974	0.73	45.49
17993	0.90	56.13
18087	0.77	47.72
18124	0.92	57.17
18160	0.84	52.32
18169	0.87	53.98
18235	0.90	55.43
18307	0.92	56.56
18332	0.92	56.69
18347	0.95	58.21
18406	0.80	49.31
18440	0.90	55.12
18458	0.89	54.48
18497	0.72	44.18
18563	0.92	55.94
18596	0.91	55.39
18620	0.89	54.29
18654	0.71	42.82
18659	0.92	55.47
18687	0.78	46.91
18705	0.91	54.95
18728	0.45	26.88
18736	0.86	51.72
18745	0.47	28.41
18796	0.91	54.45
18801	0.86	51.56
18812	0.93	55.83
18829	0.88	52.82
18876	0.83	49.46
18897	0.67	39.95
18908	0.94	56.12
18924	0.85	50.62
18944	0.88	52.39
19010	0.54	31.93
19086	0.78	46.27
19198	0.94	55.41
19200	0.88	52.09
19227	0.86	50.77
19259	0.79	46.25
19297	0.84	49.01
19316	0.89	52.25
19375	0.79	46.25
19428	0.80	46.54
19455	0.86	49.71
19500	0.73	42.30
19576	0.92	53.03
19595	0.75	43.42
19627	0.93	53.27
19749	0.87	49.82
19755	0.94	53.81
19763	0.92	52.72
19794	0.90	51.25

Table 1. (continued)

Wavenumber	Relative Feature Depth	Solar Irradiance, $\text{mW m}^{-2} \text{cm}^{-1}$
19817	0.86	49.28
19891	0.79	44.55
19949	0.92	51.93
20023	0.75	42.28
20043	0.91	51.44
20087	0.77	43.43
20106	0.90	50.41
20108	0.86	48.48
20122	0.72	40.35
20126	0.61	34.20
20133	0.82	45.66
20173	0.94	52.40
20198	0.74	41.31
20206	0.84	46.66
20221	0.93	51.97
20230	0.93	51.53
20236	0.83	46.46
20281	0.92	51.01
20329	0.63	34.92
20337	0.85	46.89
20340	0.74	40.95
20351	0.72	39.68
20367	0.81	44.86
20373	0.94	51.81
20391	0.82	45.06
20410	0.89	49.14
20422	0.86	47.37
20426	0.93	51.24
20435	0.85	46.98
20484	0.81	44.51
20610	0.83	45.23
20622	0.72	39.15
20636	0.89	48.68
20696	0.92	49.91
20698	0.93	50.21
20713	0.76	41.45
20716	0.94	50.80
20733	0.93	50.50
20779	0.86	46.50
20802	0.81	43.58
20812	0.87	46.86
20819	0.93	49.97
20827	0.78	41.98
20842	0.89	47.81
20849	0.93	49.78
20851	0.83	44.63
20854	0.85	45.81
20856	0.85	45.87
20868	0.90	48.48
20892	0.81	43.61
20908	0.77	41.41
20928	0.86	46.01
20938	0.93	49.71
20956	0.86	45.98
20962	0.91	48.67
20988	0.79	42.17
21032	0.93	49.63
21045	0.91	48.41
21058	0.82	43.32
21062	0.82	43.77
21150	0.71	37.65
21173	0.90	47.71
21195	0.83	43.60
21197	0.73	38.49
21289	0.84	44.23
21342	0.66	34.68
21380	0.77	40.24
21403	0.87	45.37
21495	0.74	38.30
21504	0.61	31.41
21524	0.76	39.16
21526	0.68	34.94

Table 1. (continued)

Wavenumber	Relative Feature Depth	Solar Irradiance, $\text{mW m}^{-2} \text{cm}^{-1}$
21581	0.75	38.43
21606	0.82	42.18
21618	0.74	37.99
21649	0.60	30.62
21683	0.81	41.61
21727	0.72	36.78
21819	0.67	33.97
21837	0.89	44.99
21955	0.93	46.60
22108	0.83	40.71
22111	0.91	44.73
22124	0.53	26.01
22148	0.90	44.33
22163	0.61	29.63
22167	0.84	41.26
22187	0.82	40.01
22190	0.93	45.77
22217	0.91	44.36
22223	0.58	28.00
22277	0.75	36.31
22289	0.90	43.61
22292	0.87	42.21
22332	0.53	25.61
22346	0.84	40.40
22454	0.75	35.72
22466	0.66	31.40
22468	0.87	41.73
22652	0.66	30.85
22657	0.69	32.01
22750	0.87	40.62
22902	0.79	36.37
22912	0.63	29.07
23162	0.71	32.20
23223	0.41	18.22
23349	0.74	33.14
23411	0.60	26.89
23471	0.48	21.55
23622	0.69	30.60
23639	0.52	22.97
23684	0.93	41.39
23719	0.66	29.03
23734	0.69	30.57
23739	0.72	31.94
23836	0.62	27.29
23884	0.64	27.94
23910	0.62	26.98
23978	0.81	35.35
23984	0.64	27.69
24015	0.66	28.54
24032	0.78	33.73
24082	0.92	39.44
24571	0.62	25.69

relative transmission of 0.95 or less. While weaker absorption features can be seen in the data for wavenumbers where the instrument's sensitivity is greatest, we adopt a uniform line strength identification threshold of 0.95 throughout for consistency, which should be adequate to determine if there is any radiatively significant discrepancy in line identification between model calculation and measurement.

We compare our normalized spectrometer measurement directly with a similarly normalized tabulation of the extraterrestrial solar irradiance (Figure 4). We find that there are 266 features in the extraterrestrial solar flux tabulation that do not appear in the spectrometer measurement. Eight such features are shown in Figure 5, and it can be seen in these two panels that the features absent from the data are conspicuous. These

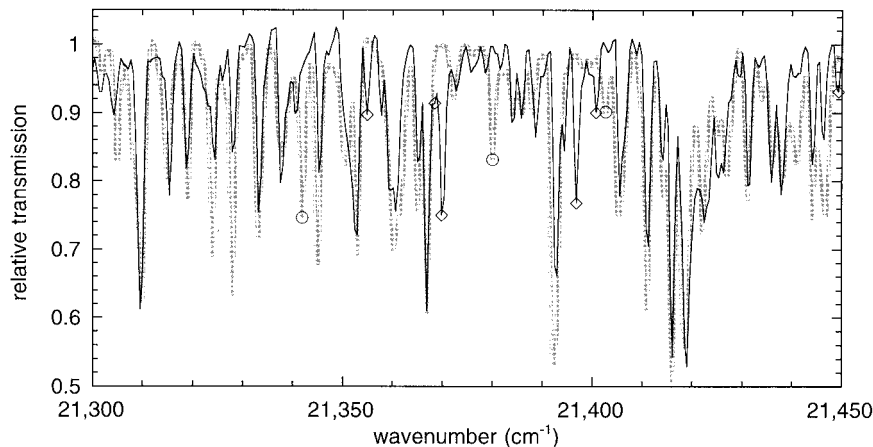


Figure 6. Examples of atmospheric absorption features seen in the spectrometer measurement which do not appear in the model spectrum. The measurement is shown by the narrow black line, and the model calculation of Figure 2 is shown by the thicker gray line. The missing absorption features are highlighted by diamonds at their local minima. The three model absorption features highlighted by circles at their local minima, which do not appear in the measured spectrum, are artifacts of unrealized solar absorption features in Table 2.

266 unrealized features are listed in Table 1. In identifying these unrealized features we have used two criteria: (1) the central minimum of the nearest feature in the spectrometer measurement is more than 1 cm^{-1} away from the tabulated feature, or (2) a concurrent feature appears in the measurement which has a relative transmission at a central minimum of greater than the threshold of 0.95 (for example, the feature at $17,170 \text{ cm}^{-1}$ in Figure 5a). This second criteria admits the possibility that an unrealized feature in the Kurucz [1992] tabulation is real but with a sizeable error in its modeled absorption strength. Such features are worth including in our tabulation because they merit further investigation. The 266 unrealized features of Table 1 represent a deficit of $\sim 1.92 \text{ W m}^{-2}$ in the Kurucz [1992] solar constant.

Performing a similar intercomparison between the measurement and the corresponding normalized direct-beam LBLRTM calculation, as in Figure 3, we find that there are 97 absorption features in the data that do not appear in the radiative transfer calculation. Five such features are shown in Figure 6, and all 97 of these features are listed in Table 2. In identifying these features as being missing from the model calculation, we have used two criteria: (1) that the measured feature have a minimum (center) relative transmission of 0.95 or less and (2) that within $\pm 1 \text{ cm}^{-1}$ of the measured feature center, there is no discernable local minimum in the model spectrum. For criterion (2), we allow a model feature of any depth (not just relative transmissions less than 0.95), because we expect any feature in the model spectrum to be the result of a discrete absorption line or cluster of absorption lines in the HITRAN-96 database. The 97 missing features of Table 2 represent a deficit in model atmospheric absorption of at most 0.23 W m^{-2} , for a solar zenith angle of 42° .

It is not straightforward to evaluate the sensitivity of this model atmospheric absorption deficit to the choice of solar zenith angle. Table 2 shows that the 97 lines are found over the entire spectral interval sampled by the FITR, over which the strength of Rayleigh scattering varies considerably. For general guidance we refer Fouquart *et al.* [1991], who intercompared the shortwave absorption of several radiative transfer models of varying spectral resolution, as part of the Intercomparison

of Radiation Codes used in Climate Models (ICRCM) project. Table 9 of Fouquart *et al.* [1991] shows that the total atmospheric absorption, for a midlatitude summer atmospheric profile, varies between ~ 84 and 206 W m^{-2} as the solar zenith angle increases from 75° to 30° . A clear-sky radiative transfer calculation using the model of Lubin *et al.* [1996] shows absorption within the ranges of Fouquart *et al.* [1991, Table 9] for both air mass extremes and further clarifies the dependence of total shortwave absorption on solar zenith angle. Specifically, we find that the total shortwave absorption increases by a factor of 1.29 as solar zenith angle decreases from 42° to 0° . Therefore as a first-order estimate, we conclude that the model absorption deficit due to the 97 missing lines should never be greater than 0.30 W m^{-2} . The model absorption deficit due to the 97 missing lines is only $\sim 0.15\%$ of the total shortwave absorption.

This study reveals that for a typical, clean maritime air mass, current knowledge of atmospheric absorption features at 1 cm^{-1} resolution is essentially complete, for application to radiative transfer modeling for climate studies. Although 97 absorption features in our data could not be conclusively identified in our LBLRTM calculation, the total radiative effect of these missing features is very small. At 1 cm^{-1} resolution, there appear to be no important unknown absorbers or poorly understood absorption bands. Using a shadow band spectroradiometer covering a similar wavelength range and having a resolution variable between 65 and 91 cm^{-1} , Mlawer *et al.* [2000] have reached similar conclusions about clear-sky excess absorption. Here we have shown that there are relatively few discrete absorption features, at 1 cm^{-1} resolution, which cannot be identified in HITRAN-96 database. Until the relatively small number of discrepancies in the Kurucz extraterrestrial solar irradiance spectrum (Table 1) are understood, the associated radiative error can be eliminated simply by removing the 266 features of Table 1 from the tabulation. Deployment of the spectrometer under a heavily contaminated troposphere [e.g., Jayaraman *et al.*, 1998] may reveal additional radiatively important absorbers not presently accounted for in HITRAN. However, for a clean air mass, radiative transfer parameterizations based upon HITRAN and current models of the ex-

Table 2. Spectral Features in the FTIR Spectrum Which Do Not Appear in the LBLRTM Direct-Beam Radiative Transfer Calculation

Wavenumber, cm ⁻¹	Relative Transmission
9310.65	0.95
9564.24	0.95
9932.58	0.89
10119.16	0.95
11717.86	0.94
11956.99	0.94
12283.38	0.89
12957.38	0.92
13248.10	0.94
14618.27	0.92
16546.26	0.88
17365.86	0.93
17524.47	0.95
17733.71	0.88
17770.84	0.91
18050.46	0.89
18166.66	0.82
18308.40	0.94
18333.95	0.93
18361.43	0.92
18622.26	0.93
18953.95	0.94
18966.01	0.83
19334.34	0.83
19570.10	0.92
19661.70	0.95
19672.79	0.95
19782.71	0.92
19927.35	0.83
19948.08	0.94
20069.57	0.95
20077.77	0.95
20109.59	0.81
20151.53	0.95
20219.51	0.95
20287.01	0.78
20306.29	0.95
20333.77	0.94
20348.24	0.93
20451.89	0.95
20462.02	0.86
20509.74	0.89
20584.96	0.87
20718.02	0.87
20897.37	0.90
20952.33	0.73
21021.27	0.86
21042.00	0.88
21071.89	0.79
21131.19	0.85
21134.09	0.94
21191.46	0.88
21294.15	0.85
21354.90	0.90
21368.39	0.92
21369.84	0.76
21396.84	0.78
21400.70	0.90
21449.39	0.94
21451.32	0.93
21480.25	0.88
21508.69	0.78
21514.96	0.82
21540.03	0.88
21660.08	0.87
21698.64	0.82
21706.84	0.77
21733.84	0.77
21745.89	0.90

Table 2. (continued)

Wavenumber, cm ⁻¹	Relative Transmission
21765.66	0.94
21802.78	0.94
21807.12	0.95
21817.25	0.94
21936.81	0.90
21957.06	0.93
21968.15	0.74
22149.91	0.89
22213.06	0.94
22323.47	0.94
22511.01	0.81
22544.76	0.82
22623.83	0.92
22816.19	0.89
22900.56	0.93
22922.74	0.91
23009.04	0.83
23056.77	0.91
23758.73	0.92
23767.41	0.94
23867.21	0.61
23894.21	0.61
24059.57	0.93
24074.04	0.90
24107.30	0.82
24153.10	0.88
24261.82	0.89
24416.82	0.80

traterrestrial solar irradiance may be used with confidence, provided that representation of continuum absorption and absorption features at coarser resolution are reliable.

Acknowledgments. This work was supported by the Ungar G. Vettlesen Foundation and by National Science Foundation funds to the Center for Clouds, Chemistry, and Climate. This report is National Science Foundation Center for Clouds, Chemistry, and Climate contribution 230.

References

- Clough, S. A., and M. J. Iacono, Line-by-line calculation of atmospheric fluxes and cooling rates, 2, Application to carbon dioxide, ozone, methane, nitrous oxide, and the halocarbons, *J. Geophys. Res.*, *100*, 16,519–16,535, 1995.
- Daniel, J. S., S. Solomon, R. W. Sanders, R. W. Portmann, D. C. Miller, and W. Madsen, Implications for water monomer and dimer solar absorption from observations at Boulder, Colorado, *J. Geophys. Res.*, *104*, 16,785–16,791, 1999.
- Fouquart, Y., B. Bonnel, and V. Ramaswamy, Intercomparing short-wave radiation codes for climate studies, *J. Geophys. Res.*, *96*, 8955–8968, 1991.
- Giver, L. P., C. Chackerian Jr., and P. Varanasi, Visible and near-infrared H₂O line intensity correction for HITRAN-96, *J. Quant. Spectrosc. Radiat. Transfer*, *66*, 101–105, 2000.
- Griffiths, P. R., and J. A. de Haseth, *Fourier Transform Infrared Spectrometry*, 656 pp., John Wiley, New York, 1986.
- Jayaraman, A., D. Lubin, S. Ramachandran, V. Ramanathan, E. Woodbridge, W. D. Collins, and K. S. Zalpuri, Direct observations of aerosol radiative forcing over the tropical Indian Ocean during the January–February 1996 pre-INDOEX cruise, *J. Geophys. Res.*, *103*, 13,827–13,836, 1998.
- Kurucz, R. L., Synthetic infrared spectra, in *Infrared Solar Physics*, edited by D. M. Rabin and J. T. Jefferies, Kluwer, Acad., Norwell, Mass., 1992.
- Lubin, D., J.-P. Chen, P. Pilewskie, V. Ramanathan, and F. P. J. Valero, Microphysical examination of excess cloud absorption in the tropical atmosphere, *J. Geophys. Res.*, *101*, 16,961–16,972, 1996.

- Michalsky, J., M. Beauharnois, J. Berndt, L. Harrison, P. Kiedron, and Q. Min, O₂-O₂ absorption band identification based on optical depth spectra of the visible and near-infrared, *Geophys. Res. Lett.*, *26*, 1581–1584, 1999.
- Mlawer, E. J., S. A. Clough, P. D. Brown, T. M. Stephen, J. C. Landry, A. Goldman, and F. J. Murcray, Observed atmospheric collision-induced absorption in the near-infrared oxygen bands, *J. Geophys. Res.*, *103*, 3859–3863, 1998.
- Mlawer, E. J., P. D. Brown, S. A. Clough, L. C. Harrison, J. J. Michalsky, P. W. Kiedron, and T. Shippert, Comparison of spectral direct and diffuse solar irradiance measurements and calculations for cloud-free conditions, *Geophys. Res. Lett.*, in press, 2000.
- Pfeilsticker, K., F. Erle, and U. Platt, Absorption of solar radiation by atmospheric O₄, *J. Atmos. Sci.*, *54*, 933–939, 1997.
- Ramanathan, V., and A. M. Vogelmann, Greenhouse effect, atmospheric solar absorption and the Earth's radiation budget: From the Arrhenius-Langley era to the 1990s, *Ambio*, *26*, 38–46, 1997.
- Solomon, S., R. W. Portmann, R. W. Sanders, and J. S. Daniel, Absorption of solar radiation by water vapor, oxygen, and related collision pairs in the Earth's atmosphere, *J. Geophys. Res.*, *103*, 3847–3858, 1998.
- Solomon, S., R. W. Portmann, R. W. Sanders, J. S. Daniel, W. Madsen, B. Bartram, and E. G. Dutton, On the role of nitrogen dioxide in the absorption of solar radiation, *J. Geophys. Res.*, *104*, 12,047–12,058, 1999.
- Stephens, G. L., and S.-C. Tsay, On the cloud absorption anomaly, *Q. J. R. Meteorol. Soc.*, *116*, 671–704, 1990.
- Rothman, L. S., et al., The HITRAN Molecular Spectroscopic Database and HAWKS (HITRAN Atmospheric Workstation): 1996 edition, *J. Quant. Spectrosc. Radiat. Transfer*, *60*, 665–710, 1998.
- Zender, C. S., Global climatology of abundance and solar absorption of oxygen collision complexes, *J. Geophys. Res.*, *104*, 24,471–24,484, 1999.
-
- J. Ebrahimian, Biospherical Instruments, Inc., San Diego, CA 92110.
A. Kressin, Department of Chemistry, Miramar College, San Diego, CA 92126.
P. J. Lehr, Space Sciences Laboratory, University of California, Berkeley, CA 92740.
D. Lubin, V. Ramanathan, and A. Vogelmann, Scripps Institution of Oceanography, University of California, 9500 Gilman Drive, La Jolla, CA 92093-0221. (dlubin@ucsd.edu)

(Received December 8, 1999; revised April 25, 2000; accepted May 5, 2000.)